Int. J. Electrochem. Sci., 8 **(2013)** 6535 - 6543

International Journal of
ELECTROCHEMICAL
SCIENCE
www.electrochemsci.org

Synthesis of Double-Shelled $LiMn_2O_4$ Hollow Microspheres with Enhanced Electrochemical Performance for Lithium Ion Batteries

Shuquan Liang, Juan Yi and Anqiang Pan[*]

School of Materials Science and Engineering, Central South University, Changsha, 410083, China
[*]E-mail: pananqiang@gmail.com

Received: 3 March 2013 / *Accepted:* 22 March 2013 / *Published:* 1 May 2013

Double-shelled $LiMn_2O_4$ hollow microspheres have been prepared from hydrothermally synthesized urchin-like α-MnO_2 spheres. A large hollow interior and broad gap between exterior and interior shells are clearly observed within the hollow microspheres. Moreover, the exterior shell is composed of octahedron-shaped nanoparticles. For comparison, $LiMn_2O_4$ are also prepared using commercial MnO_2 particles as starting material. As a cathode material for LIBs, it exhibit superior rate capability and cyclic stability. A specific discharge capacity of 126 mA h g^{-1} can be obtained at 0.2 C in the voltage range of 3-4.3 V, which retains 96.5% of its original discharge capacity even after 100 cycles. The good electrochemical performance is attributed to the double-shelled structures of the $LiMn_2O_4$.

Keywords: Double-shelled, Hollow microspheres, Manganese dioxide, $LiMn_2O_4$, Lithium-ion batteries

1. INTRODUCTION

Lithium ion batteries (LIBs) are currently the dominating power sources for advanced portable electronic devices and have been under serious consideration to power the next generation of electric vehicles (EVs) and hybrid electric vehicles (HEVs).[1-4] Spinel $LiMn_2O_4$ is one of the most promising cathode materials for LIBs because of its low cost, environmental benign and good safety.[5-10] However, it still suffers from the two main drawbacks before their success in large scale production for HEVs and EVs: (1) the rapid decrease of capacity upon cycling caused by the presence of acid solution and the Jahn-Teller effect;[11-13] (2) and the low diffusion coefficient in solid $LiMn_2O_4$ phase (10^{-8}-10^{-10}).[11, 14] It is well known that nanostructured materials can mitigate such problems because of the shortened Li^+ ions diffusion distance and the reduced stress upon cycling.[15] Therefore various

methods have been explored to synthesize nanostructured $LiMn_2O_4$, such as nanoparticles,[16, 17] one-dimensional nanomaterials (nanowires,[18, 19] nanorods,[5] and nanotubes[6]), mesoporous materials[20, 21] and nano-crystalline thin films.[22] It is found the electrochemical performances are largely dependent on the morphology, the crystallinity and the porosity of the structures.

In the last decade, hollow micro-/nanomaterials have attracted considerable attention in the field of LIBs due to their structural advantages.[23, 24] The nano-sized subunits can significantly provided a reduced Li^+ ions diffusion distance and enlarged electrode-electrolyte contact area, leading to good rate capability. Moreover, the hollow interiors can well accommodate the volume change and alleviate the strain upon cycling.[25] To date, hollow structures with diversified composition have been fabricated and used in lithium ion batteries, such as TiO_2,[26] SnO_2[27, 28] and V_2O_5.[29, 30] However, the synthesis of hollow structures for lithium transition metal oxides or phosphates, are much less reported, probably due to the high lithiation temperature.

Because of the particular feature of hollow structures, $LiMn_2O_4$ hollow microspheres have been successfully prepared, presenting their attractive performance for LIBs.[31-35] Luo et al. reported the preparation of $Li_{1.05}Mn_2O_4$ hollow spheres by chemical lithiation of MnO_2 hollow spheres with LiI.[31] Xiao et al. found that $LiMn_2O_4$ hollow microspheres exhibit better rate capability.[34] However, the synthesis of $LiMn_2O_4$ with more complex structures is much less reported. Ding et al. has successfully prepared double-shelled $LiMn_2O_4$ microspheres using $MnCO_3$ spheres as sacrifice templates, which show good rate capability.[32] However, to date, no double-shelled $LiMn_2O_4$ microspheres are reported directly using MnO_2 as the templates, which is more common and cost-effective.

Herein, we report the successfully preparation of double-shelled $LiMn_2O_4$ hollow microspheres from the hydrothermal prepared hierarchical α-MnO_2 hollow microspheres. As cathode materials for lithium ion batteries, the double-shelled $LiMn_2O_4$ hollow microspheres exhibit improved rate capability and good cyclic stability.

2. EXPERIMENTAL PART

Synthesis of hierarchical MnO_2 hollow microspheres: In a typical synthesis, 2 mmol $MnSO_4$, 2 mmol $K_2S_2O_8$ and 0.01mmol $AgNO_3$ were dissolved in 50 ml distilled water, and then 2 mL concentrated sulfuric acid was dripped into the above mixture solution. After standing at room temperature for three days, the precipitates were filtered off and washed with distilled water and absolute ethanol for several times. The as-obtained materials were dried in an oven at 60 ^oC overnight to get the final MnO_2 hollow microspheres (designated as S-MO).

Synthesis of spinel $LiMn_2O_4$ double-shelled hollow microspheres: The pre-synthesized MnO_2 hierarchical hollow microspheres and LiOH in a molar ratio of 2:1 were mixed together in a mortar, which was annealed firstly in a muffle furnace at 360 ^oC for 4 h，then treated at 750 ^oC for another 12 h to get the double-shelled $LiMn_2O_4$ hollow microspheres (designated as S-LMO). For comparison, $LiMn_2O_4$ (designated as C-LMO) was also prepared from commercial MnO_2 (designated C-MO), keeping other parameters unaltered.

Structural Characterizations: The phase purity of the as-prepared products was studied by X-ray power diffraction (XRD, Rigaku D/max2500). The morphologies and sizes of the as-prepared products were characterized by scanning electron microscopy (SEM, FEI Nova NanoSEM 230). High-resolution transmission electron microscope (HRTEM) analysis was performed on the JEOL JEM-2100F transmission electron microscope.

Electrochemical measurements: The electrochemical properties were evaluated in coin cells (CR 2016). $LiMn_2O_4$, acetylene black and polyvinylidene fluoride (PVDF) binder in a weight ratio of 70∶20∶10 were mixed and dispersed in N-methyl-2-pyrrolidone (NMP) solution to make the slurry, which was coated on aluminum foil and dried in a vacuum oven at 100 ^oC for 10 h prior coin-cell assembling. The $LiMn_2O_4$/Li half cells (2016 type coin cells) were assembled in a glove box (Mbraun, Germany) filled with ultra-high purity argon using polypropylene membrane as the separator, Li metal as the anode, and 1-M $LiPF_6$ in ethylene carbonate/dimethyl carbonate(EC/DMC) (1∶1 v/v) as the electrolyte. The galvanostatic charge/discharge performances of the electrodes were evaluated at room temperature using an Land Battery Tester (Land CT 2001A) in the voltage range of 3 V- 4.3 V (vs. Li/Li^+). The impedance spectrometry (EIS) was obtained on a ZAHNER-IM6ex electrochemical workstation (ZAHNER Co., Germany).

3. RESULTS AND DISCUSSIONS

The crystallinity of S-MO and C-MO were characterized by XRD and the results are shown in Fig. 1a. The peak positions of the XRD patterns are almost the same for the two samples and can be well indexed to a tetragonal phase of α-MnO_2 (JCPDS 44-0141).[31, 36] No other phases are detected, which indicates the high purity of the as-synthesized products. However, the diffraction peaks for S-MO is much broader than those for C-MO, which can be attributed to the lower crystallinity and smaller crystallites for S-MO samples. Figure 1b shows a typical scanning electron microscopy (SEM) image of urchin-like hierarchical MnO_2 microspheres prepared by hydrothermal method. The morphologies of the as-prepared samples are quite uniform in a size ranging from 2.5 μm to 4 μm. The enlarged SEM image (Figure 1c) shows the microspheres is composed of rod-like subunits, which grow vertically on the surface and leave a large space between neighboring nanorods. The hierarchical MnO_2 microspheres are further characterized by transmission electron microscopy (TEM) and high resolution transmission electron microscopy (HRTEM). As shown in Figure 1e, the hollow interior can be observed, although the diameter of the interior shell is only about 200 nm. The MnO_2 nanorods can be of several micrometers in length. The HRTEM image (shown in Figure 1f) of a single nanorod reveals the nanorods are about 20 nm in diameter and the nanorod is a single crystal. Moreover, a thin amorphous layer is detected on the surface of the nanorods. The morphologies of the purchased MnO_2 (C-MO) are also shown in Figure 1d, which indicates the sub-micron sized MnO_2 octahedral crystals are densely agglomerated and the particles around 400 nm are much larger than the subunits of MnO_2 nanorods.

The phases of the calcinations products are determined by XRD to be face-centered cubic $LiMn_2O_4$ [JCPDS No. 35-0782, space group: $Fd\bar{3}m$ (no.227)] and no other phases were detected,

demonstrating the high purity of the synthesized $LiMn_2O_4$.[5, 32] As shown in Figure 2, no distinct peak position difference has been observed.

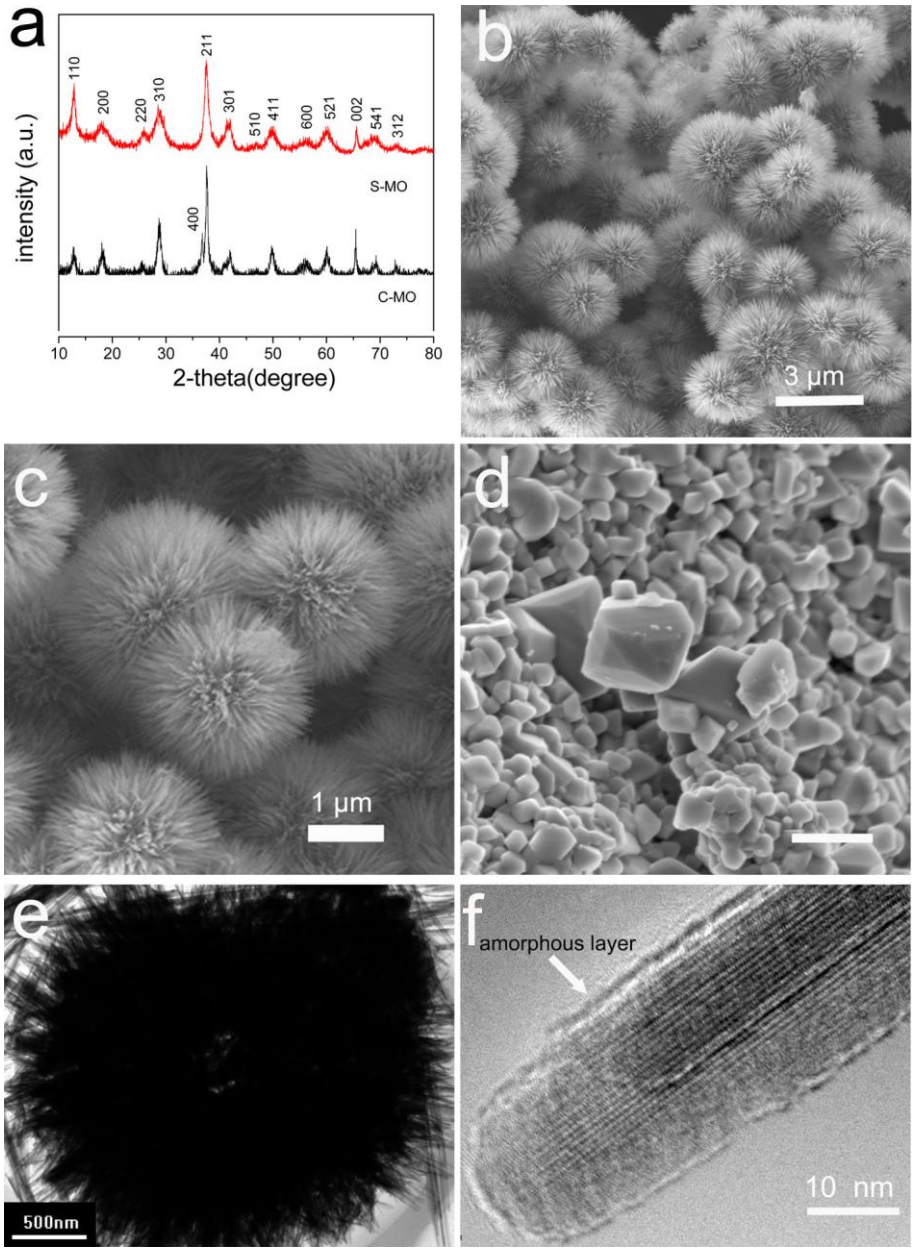

Figure 1. XRD patterns for S-MO and C-MO (a), SEM images for S-MO (b, c) and C-MO (d), TEM images (e, f) for S-MO.

Whereas the peak intensity of (111) face is much stronger for C-LMO, which can be attributed to their higher crystallinity. It is well known that the intensity ratio of the (311)/(400) peaks reflects the degree of tetragonal distortion from the cubic spinel structure.[37] As shown in Figure 2, the peak intensity ratio of (311) to (400) for S-LMO is lower than that for C-LMO. Therefore, $LiMn_2O_4$ with different tetragonal distortion rate can be obtained from using diversified starting materials.

The structures of the as-fabricated $LiMn_2O_4$ samples after lithiation and annealing in air at 750 ^oC for 12 h are characterized by SEM and TEM, and the results are shown in Figure 3. As shown in Figure 3a, the urchin-like nanorods have changed their morphologies from the long uniform nanorods to octahedron-shaped nanoparticles, which stack together to form the hierarchical $LiMn_2O_4$ microspheres with similar diameter to that of MnO_2 precursor microspheres.

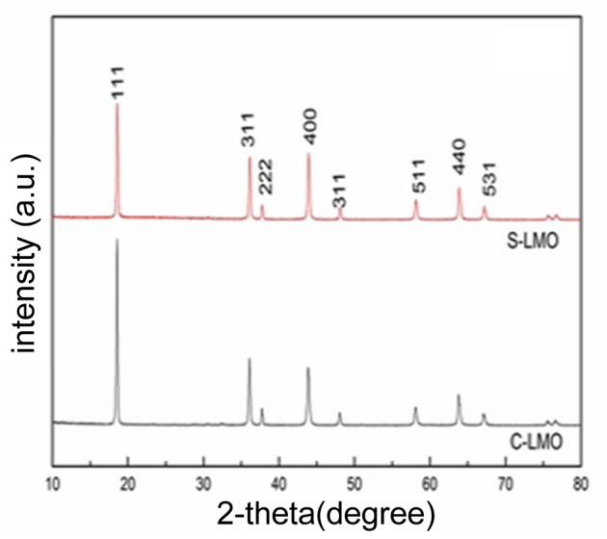

Figure 2. XRD patterns for S-LMO and C-LMO.

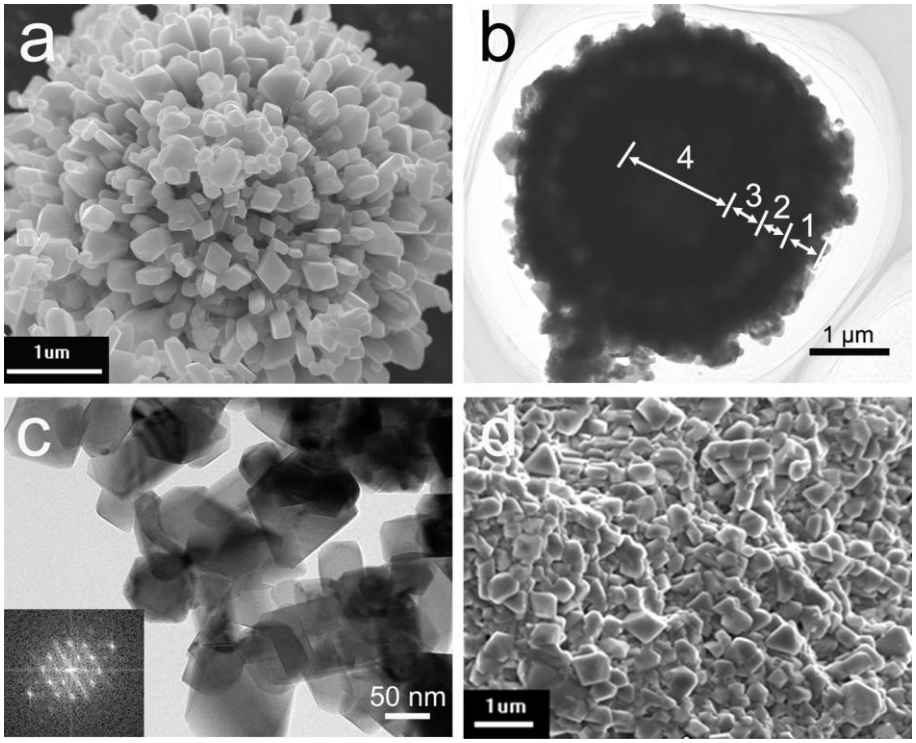

Figure 3. The SEM (a), TEM images (b, c) of the double-shelled $LiMn_2O_4$ hollow microspheres; and the SEM images (d) of the $LiMn_2O_4$ prepared from commericial MnO_2.

The interior structures of the $LiMn_2O_4$ microspheres are further studied by TEM, which reveals the $LiMn_2O_4$ is of double-shelled hollow structures (see Figure 3b). As indicated by '1' and '3' in the Figure 3b, the exterior and interior shells are about 460 nm and 430 nm in thickness, respectively. And a broad empty gap in a size of 340 nm is observed between the exterior and interior shells (indicated by '2'). Moreover, the interior microsphere is hollow-structured with a diameter around 1.42 μm (indicated by '4').

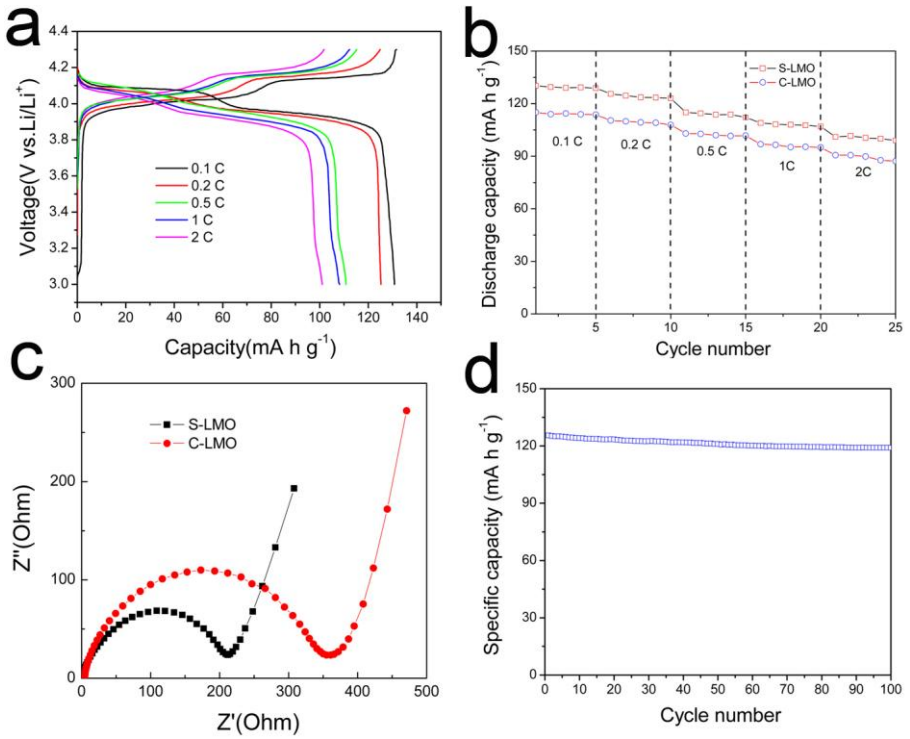

Figure 4. Discharge/charge curves for S-LMO electrodes at different current densities (a) and rate performance for both S-LMO and C-LMO electrodes (b), Nyquist plots for S-LMO and C-LMO electrodes (c), and cycling performance (d) of S-LMO in the voltage range of 3-4.3 V at a rate of 0.2 C.

The formation of double-shelled hollow microspheres can be explained by the kinetics of the lithiation process during calcinations. As shown in Figure 1c and 1e, the MnO_2 microspheres are composed of nanorods of several micrometers and the hollow interior is quite small. It is believed that the exterior MnO_2 nanorods can react with LiOH more efficiently to form octahedron-shaped $LiMn_2O_4$. However, the MnO_2 located inside can not transferred into $LiMn_2O_4$ at the same time due to the limitation of oxygen and lithium sources diffusion. To complete the transformation, the interior MnO_2 materials move outside and react with incoming LiOH, thus results a larger hollow interior. The formation of the hollow interior is quite similar to the preparation of hollow $LiNi_{0.5}Mn_{1.5}O_4$ microspheres, which use $MnCO_3$ sacrifice microspheres, $Ni(NO_3)_2$ and LiOH.[38]

Figure 3c shows the exterior shells are composed of loosely compacted octahedron nanoparticles ranging from 50 nm to 100 nm. The FFT image (see inset of Figure 3c) indicates the octahedron nanoparticles are of a single crystal. Figure 3d shows the SEM image of the $LiMn_2O_4$

particles prepared from the commercial MnO_2. It is clearly observed that the particles are of a larger size about 500 nm and are more densely compacted. The results demonstrate that the morphologies of the starting MnO_2 have a great effect on the final morphologies of the annealed samples.

The electrochemical performance of S-LMO and C-LMO are evaluated and the results are shown in Figure 4. Figure 4a shows the discharge/charge profiles of the S-LMO electrode at different rates. Two plateaus at 4.0 and 4.1 V on the charge curve are well observed, which indicates the two-step lithium ions removal process and the phase evolute from $LiMn_2O_4$ to $Li_{0.5}Mn_2O_4$ and λ-MnO_2.[6] The observation of two corresponding plateaus on the discharge curve demonstrates the good structural reversibility of S-LMO electrodes and the results are related well with the previous reports.[35, 39, 40] The plateaus are all well displayed for all the profiles, indicating the good rate performance of the S-LMO electrode. Figure 4b compares the rate capability of S-LMO and C-LMO electrodes in the voltage range of 3-4.3 V. For the S-LMO electrode, it delivers specific discharge capacities of 130, 125, 118, 109 and 101 mA h g^{-1} at 0.1, 0.2, 0.5, 1 and 2 C, respectively. In contrast, C-LMO electrode only presents a specific capacity of 116 mA h g^{-1} at 0.1 C and retains a capacity of 87.8 mA h g^{-1} at 2 C. The electrochemical impedance spectra (EIS) of S-LMO and C-LMO electrodes are shown in Fig.4b. The charge transfer resistance of S-LMO (ca.210 Ω) is much lower than that of C-LMO (ca.360 Ω), demonstrating superior dynamics for lithium ions insertion and removal process in S-LMO electrode. The rate performance is even better than that of hollow $LiMn_2O_4$ microcubes.[33] The superior performance for S-LMO can be attributed to the novel double-shelled hollow structures. The nanosized octahedron particles can reduce the lithium ions diffusion and electron transportation distance, and the hollow interior and the gap between the double shells can increase the contact area between electrode and electrolyte, thus allowing better rate capability and easier charge transfer. The cycling performance of S-LMO electrode is also measured at a rate of 0.2 C in the voltage range of 3.0 and 4.3 V (see Figure 4d). An initial specific discharge capacity of 126 mA h g^{-1} can be delivered for S-LMO electrode, and it still retains a specific discharge capacity of 119 mA h g^{-1} even after 100 cycles, maintaining 95.6% of its original capacity. The capacity fading rate is only 0.05 % per cycle. The results demonstrate that the double-shelled $LiMn_2O_4$ hollow microspheres have very good cyclic stability, which can be attributed to the easier accommodation to the volume and stress change upon cycling. The cycling performance is also superior to many other LMO. [41-43] This good cycle performance can be attributed to the advantages of double-shelled hollow $LiMn_2O_4$ microspheres, including reducing the Li^+ ions diffusion and electron transportation distance, increasing the electrode and electrolyte contact area and accommodating the volume, stress change upon cycling.

In summary, double-shelled $LiMn_2O_4$ hollow microspheres have been successfully fabricated from hydrothermal prepared hierarchical urchin-like MnO_2 microspheres. The as-obtained $LiMn_2O_4$ microspheres have a large hollow interior and an obvious gap between the double shells. As a cathode material for lithium ion batteries, it exhibits superior rate capability and cyclic stability. A specific discharge capacity of 125 mA h g^{-1} can be delivered at 0.2 C, which retains 119 mA h g^{-1} after 100 cycles with a capacity retention of 95.6%. The superior electrochemical performances of S-LMO are attributed to the novel double-shelled hollow $LiMn_2O_4$ microspheres: (1) the nanosized subunits of the microspheres provide shortened Li^+ diffusion and electron transportation distance; (2) the hollow interior and the large gap between the double shells can increase the contact area between electrode

and electrolyte; (3) moreover, the hollow structures within the microspheres can easier accommodate the volume and stress change during cycling. The results demonstrate the double-shelled hollow $LiMn_2O_4$ microspheres are promising electrode materials for LIBs.

ACKNOWLEDGMENTS
This work was supported by National High Technology and Development Program 863 (2013AA110106), Science Fund for Creative Research Groups of the National Natural Science Foundation of China (Grant No. 50721003) and Lie-Ying Program of Central South University.

References

1. J.M. Tarascon and M. Armand, *Nature* 414 (2001) 359.
2. M.S. Whittingham, *Chem. Rev*. 104 (2004) 4271.
3. K. Kang, Y.S. Meng, J. Berger, C.P. Grey and G. Ceder, *Science* 311 (2006) 977.
4. A.Q. Pan, J.G. Zhang, Z.M. Nie, G.Z. Cao, B.W. Arey, G.S. Li, S.Q. Liang and J. Liu, *J. Mater. Chem.* 20 (2010) 9193.
5. D.K. Kim, P. Muralidharan, H.W. Lee, R. Ruffo, Y. Yang, C.K. Chan, H. Peng, R.A. Huggins and Y. Cui, *Nano Lett*. 8 (2008) 39484.
6. Y.-L. Ding, J. Xie, G.-S. Cao, T.-J. Zhu, H.-M. Yu and X.-B. Zhao, *Adv. Funct. Mater*. 21 (2011) 348.
7. M.M. Thackeray, W.F. David, P.G. Bruce and J.B. Goodenough, *Mater. Res. Bull*. 18 (1983) 481.
8. D. Guyomard and J.M. Tarascon, *J. Electrochem. Soc*. 139 (1992) 937.
9. Y.Y. Xia and M. Yoshio, *J. Electrochem. Soc*. 144 (1997) 4186.
10. S.H. Park, K.S. Park, Y.K. Sun and K.S. Nahm, *J. Electrochem. Soc.* 147 (2000) 2166.
11. O. Park, Y. Cho, S. Lee, H. Yoo, H. Song and J. Cho, *Energy Environ. Sci*. 4 (2011) 1621.
12. P.G. Bruce, B. Scrosati and J.M. Tarascon, *Angew. Chem. Int.* Ed. 47 (2008) 2930.
13. G. Amatuccia and J.M. Tarascon, *J. Electrochem. Soc*. 149 (2002) K31.
14. J. Xie, T. Tanaka, N. Imanishi, T. Matsumura, A. Hirano, Y. Takeda and O. Yamamoto, *J. Power Sources* 180 (2008) 576.
15. A. Arico, P. Bruce, B. Scrosati, J.M. Tarascon and V. Schalkwijik, *Nature Mater*. 4 (2005) 366.
16. C.J. Curtis and J. Wang, *J. Electrochem. Soc*. 151 (2004) 590.
17. M. Okubo, E. Hosono, J. Kim, M. Enomoto, N. Kojima, T. Kudo, H.S. Zhou and I. Honma, *J. Am. Chem. Soc.* 129 (2007) 7444.
18. E. Hosono, T. Kudo, I. Honma, T. Matsumura and H.S. Zhou, *Nano Lett*. 9 (2009) 1045.
19. L.Z. Zhang, J.C. Yu, A.W. Xu, Q. Li, K.W. Kwong and L. Wu, *Chem. Commun*. (2003) 2910.
20. F. Jiao, J. Bao, A.H. Hill and P.G. Bruce, *Angew. Chem. Int. Ed*. 47 (2008) 9711.
21. J.-Y. Luo, Y.G. Wang, H.-M. Xiong and Y.Y. Xia, *Chem. Mater*. 19 (2007) 4791.
22. S.B. Tang, M.O. Lai and L. Lu, *Electrochim. Acta* 52 (2006) 1161.
23. X.W. Lou, L.A. Archer and Z.C. Yang, *Adv. Mater.* 20 (2008) 3987.
24. X.Y. Lai, J.E. Halpert and D. Wang, *Energy Environ. Sci*. 5 (2012) 5604.
25. Z.Y. Wang, L. Zhou and X.W. Lou, *Adv. Mater.* 24 (2012) 1903.
26. S.J. Ding, J.S. Chen, Z.Y. Wang, Y.L. Cheah, S. Madhavi, X.A. Hu and X.W. Lou, *J. Mater. Chem.* 21 (2011) 1677.
27. X.W. Lou, Y. Wang, C.L. Yuan, J.Y. Lee and L.A. Archer, *Adv. Mater.* 18 (2006) 2325.
28. S.J. Ding, J.S. Chen, G.G. Qi, X.N. Duan, Z.Y. Wang, E.P. Giannelis, L.A. Archer and X.W. Lou, *J. Am. Chem. Soc.* 133 (2011) 21.
29. A.Q. Pan, H.B. Wu, L. Yu and X.W. Lou, *Angew. Chem. Int. Ed*. 52 (2013) 2226.
30. A.Q. Pan, T. Zhu, H.B. Wu and X.W. Lou, *Chemisty-A European Journal* 19 (2013) 494.
31. J.-Y. Luo, L. Cheng and Y.Y. Xia, *Electrochem. Commun*. 9 (2007) 1404.

32. Y.-L. Ding, X.-B. Zhao, J. Xie, G.-S. Cao, T.-J. Zhu, H.-M. Yu and C.Y. Sun, *J. Mater. Chem*. 21 (2011) 9475.
33. Y.M. Wu, Z.H. Wen, H.B. Feng and J.H. Li, *Small* 8 (2012) 858.
34. X.L. Xiao, J. Lu and Y. D. Li, *Nano Res.* 3 (2010) 733.
35. L. Zhou, X.F. Zhou, X.D. Huang, Z.P. Liu, D.Y. Zhao, X.D. Yao and C.Z. Yu, *J. Mater. Chem*. A 1 (2013) 837.
36. X. Wang and Y.D. Li, *Chem. Commun.* (2002) 764.
37. M. Tabuchi, C. Masquelier, H. Kobayashi, R. Kanno, Y. Kobayashi, T. Akai, Y. Maki, H. Kageyama and O. Nakamura, *J. Power Sources* 68 (1997) 623.
38. L. Zhou, D. Y. Zhao, X. W. Lou, *Angew. Chem. Int. Ed.* 51 (2012) 239.
39. J.-Y. Luo, H.-M. Xiong, Y. Y. Xia, J. Phys. Chem. C 112 (2008) 12051.
40. C.Y. Sun, H.Y. Yang, J. Xie, G.-S. Cao, X.-B. Zhao, T.J. Zhu, *Int. J. Electrochem. Sci.* 7 (2012) 6191.
41. X. Li, F. Cheng and B. Guo, J. Chen, *J. Phys. Chem.* B 109 (2005) 14017.
42. W.-H. Ryu, J.-Y. Eom, R.-Z. Yin, D.-W. Han, W.-K. Kim and H.-S. Kwon, *J. Mater. Chem*. 21 (2011) 15337.
43. D. Arumugam, G.P. Kalaignan, K. Vediappan and C.W. Lee, *Electrochim. Acta* 55 (2010) 8439.